# Glutathione-dependent redox balance characterizes the distinct metabolic properties of follicular and marginal zone B cells

D. G. Franchina *et al.*

Supplementary Figure 1. Exemplary gating of the main strategies for flow cytometry and cell sorting.

a

MFI	Fig. or Supp.
DCFDA	1c; 2f; S2a
MitoSOX	1d; 2g; S2b
MBB	1e; S3g; S6g
p-mTOR	3b; 3e
p-S6	3c; 3f
PIP3	3g
2-NBDG	4b; 4f
Glut-1	4c; 4g
MT-Red	5k
MT-Green	5k
Sdha	5m
BODIPY C11	S2d
ICAM-1	S3a
VCAM-1	S3a
ER-Tracker	S5b, g
Giantin	S5b, g
p-eIF4E	S5c, h
Puromycin	S5f, k
Hexokinase-1	S6b
TNP	S7a

b
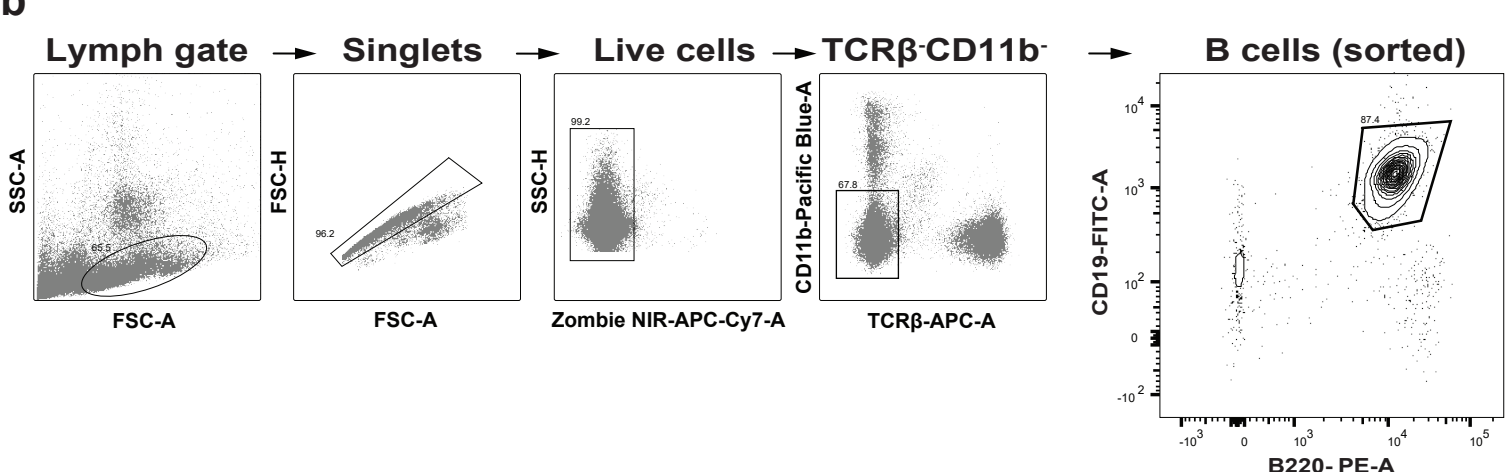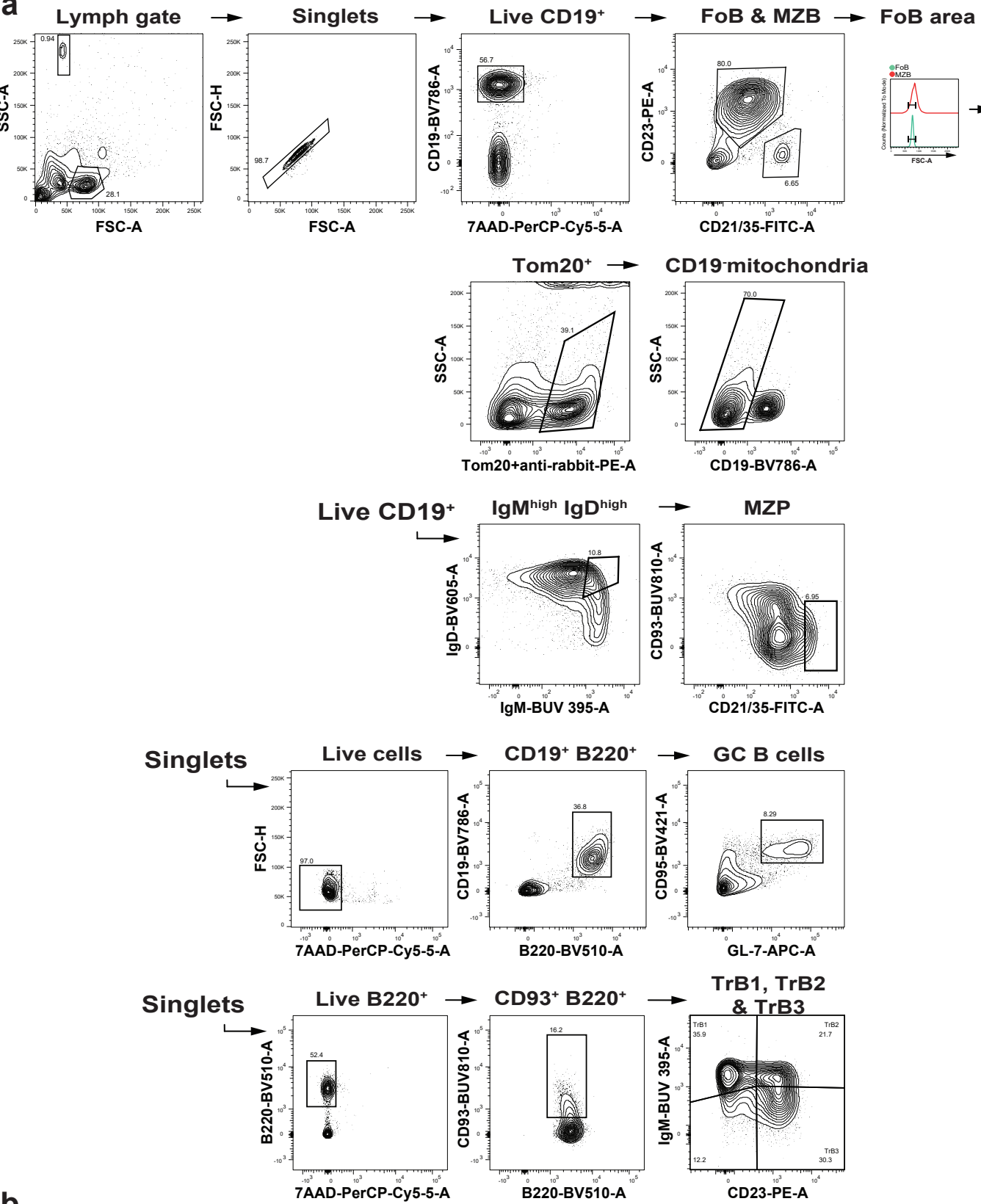
Supplementary Figure 1. Exemplary gating of the main strategies for flow cytometry and sorting.

(**a**). General and representative flow cytometry gating strategy for gating of FoB, MZB, Tom20$^+$ mitochondria, MZP, GC B cells, transitional B cells (TrB1, TrB2 and TrB3). For mean fluorescence intensity (MFI) measurements, signal from the MZB gate was size-corrected based on the FSC-A signal from FoB as shown (**b**). Flow cytometry back-gating strategy for sorting splenic B cells for scRNA-sequencing. Numbers in contour plots represent percentages of the cells gated.

Supplementary Figure 2. *Gclc* deletion led to ROS increase in splenic B cells and loss of MZB, which is *Cre*-independent.
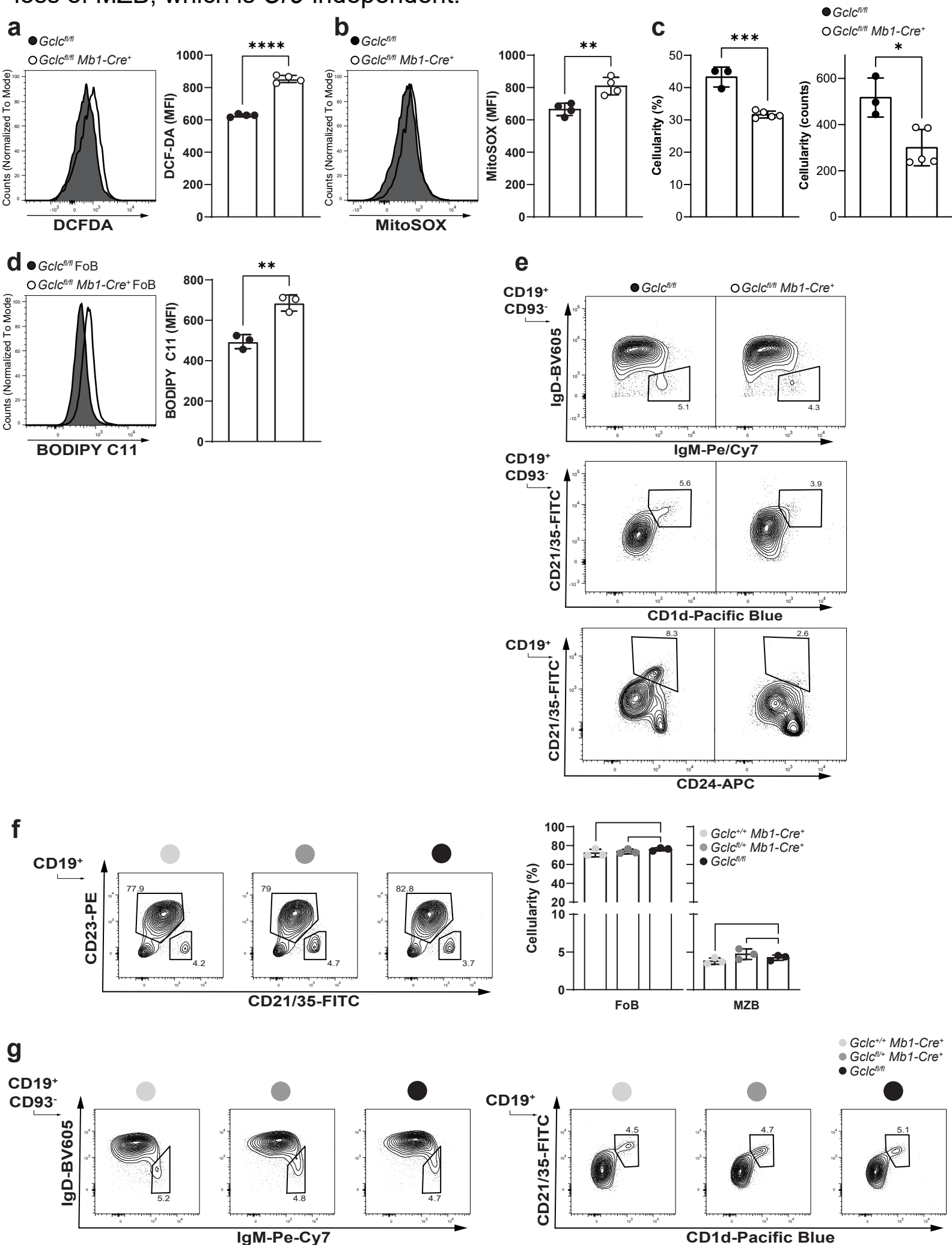
Supplementary Figure 2. *Gclc* deletion led to ROS increase in splenic B cells and loss of MZB, which is *Cre*-independent.

(a-b) Representative histogram (left) and quantitation (right) of DCFDA staining for intracellular ROS and MitoSOX for mitochondrial ROS detection in total splenic CD19$^+$ B cells from *Gclc$^{fl/fl}$* and *Gclc$^{fl/fl}$ Mb1-Cre$^+$* mice (gated as in Supplementary Figure 1a) (n = 4 animals examined over 3 independent experiments). **(c)** Percentages (left) and absolute numbers (right) of viable splenic CD19$^+$ cells from *Gclc$^{fl/fl}$* and *Gclc$^{fl/fl}$ Mb1-Cre$^+$* mice (gated as in Supplementary Figure1a) (n = 3-5 animals examined over 3 independent experiments). **(d)** Representative histogram (left) and quantitation (right) of BODIPY C11 staining for lipid ROS detection in splenic FoB cells from *Gclc$^{fl/fl}$* and *Gclc$^{fl/fl}$ Mb1-Cre$^+$* mice (gated as in Supplementary Figure 1a) (n = 3 animals examined over 2 independent experiments). **(e)** Representative contour plots of the expression of the indicated MZB markers gated as indicated from total splenocytes of *Gclc$^{fl/fl}$* and *Gclc$^{fl/fl}$ Mb1-Cre$^+$* mice. **(f)** Representative FACS contour plot (left) and quantitation (right) of splenic FoB and MZB from *Gclc$^{+/+}$ Mb1-Cre$^+$*, *Gclc$^{fl/+}$ Mb1-Cre$^+$* and *Gclc$^{fl/fl}$ Mb1-Cre$^-$* mice (gated as in Supplementary Figure 1a) (n = 3 animals examined over 2 independent experiments). **(g)** Representative contour plots of the indicated MZB markers expressed by total splenocytes of *Gclc$^{+/+}$ Mb1-Cre$^+$*, *Gclc$^{fl/+}$ Mb1-Cre$^+$* and *Gclc$^{fl/fl}$* mice. In contour plots numbers represent percentages of the cells gated. Data are the mean ± SD. Each dot represents one mouse. Significance (P) was calculated with unpaired t-test, except for (f) (one-way ANOVA). *: P ≤ 0.5; **: P ≤ 0.01; ***: P ≤ 0.001; ****: P ≤ 0.0001.

Supplementary Figure 3. Loss of MZB content in *Gclc*-deficient mice is due to defective maturation of B cell precursors.
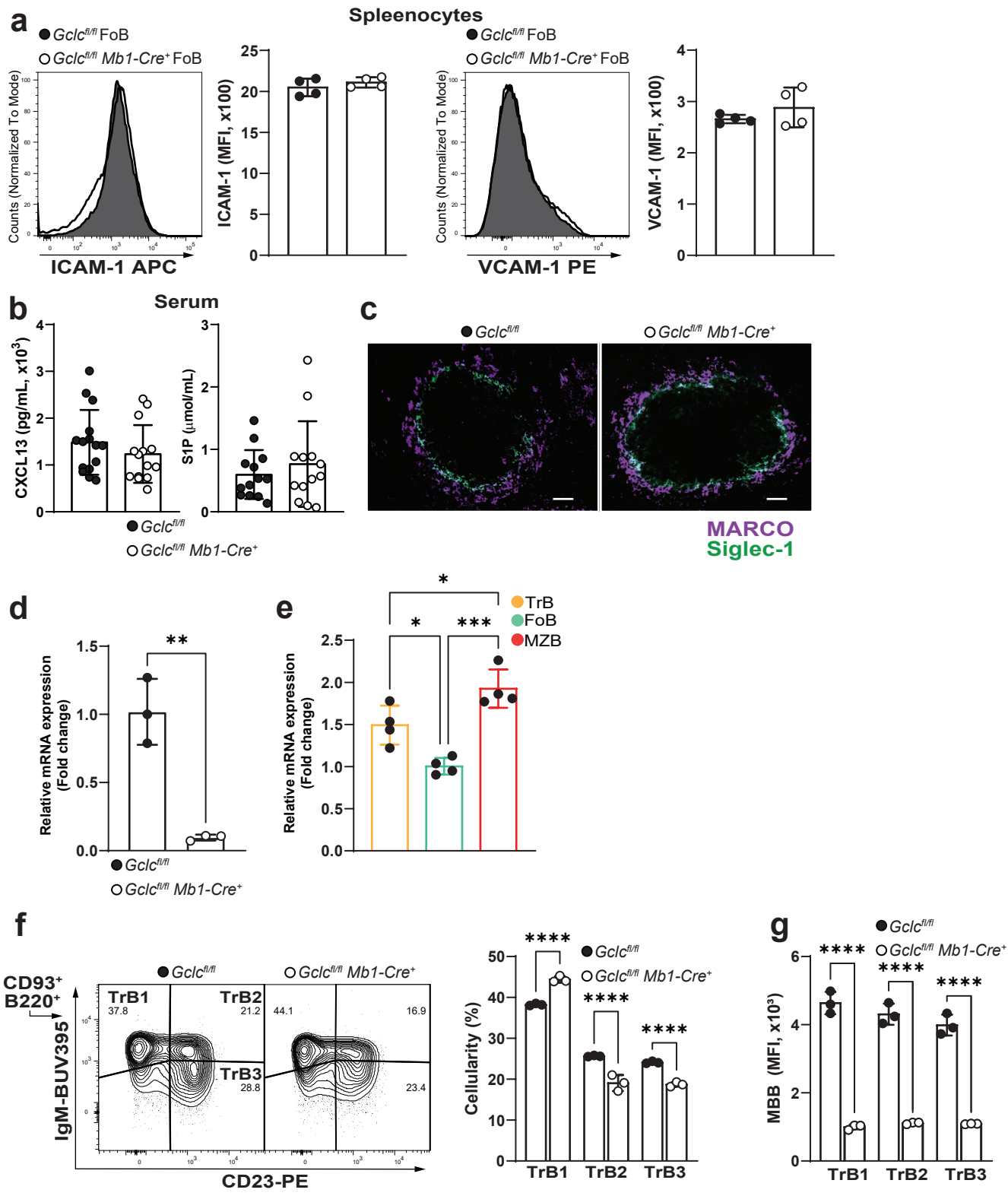
Supplementary Figure 3. Loss of MZB content in *Gclc*-deficient mice is due to defective maturation of B cell precursors.

(**a**) Representative histogram (left) and MFI statistic of ICAM-1 and VCAM-1 staining in total live splenocytes from *Gclc*$^{fl/fl}$ and *Gclc*$^{fl/fl}$ *Mb1-Cre*$^+$ mice (n = 4 animals examined over 3 independent experiments). (**b**) ELISA quantitation of CXCL13 and S1P from serum of *Gclc*$^{fl/fl}$ and *Gclc*$^{fl/fl}$ *Mb1-Cre*$^+$ mice (n = 3-5 animals examined over 4 independent experiments; data are pooled from 3 experiments). (**c**) Representative immunofluorescence staining to detect MARCO$^+$ metallophilic macrophages (purple) and Siglec-1$^+$ marginal zone macrophages (green) in a single spleen follicle resected from one *Gclc*$^{fl/fl}$ and one *Gclc*$^{fl/fl}$ *Mb1-Cre*$^+$ mouse. Scale bars: 50 µm. (**d-e**) RT-qPCR of *Gclc* mRNA expression in resting total sorted CD93$^+$ TrB from spleen of splenocytes from *Gclc*$^{fl/fl}$ and *Gclc*$^{fl/fl}$ *Mb1-Cre*$^+$ mice (d) and from resting FoB (green), MZB (red) and TrB (orange) isolated from spleen of B6 mice (e) (n = 3 animals examined over 2 independent experiments). (**f**) Representative contour plot (left) and percentages (middle) statistic of Trb1-3 from *Gclc*$^{fl/fl}$ and *Gclc*$^{fl/fl}$ *Mb1-Cre*$^+$ mice (gated as in Supplementary Figure 1a) (n = 3 animals examined over 3 independent experiments). (**g**) Mean fluorescence intensity (MFI) of MBB staining for detection of intracellular thiols from the cells gated in (f) from *Gclc*$^{fl/fl}$ and *Gclc*$^{fl/fl}$ *Mb1-Cre*$^+$ mice (n = 3 animals examined over 2 independent experiments). In contour plots numbers represent percentages of the cells gated. Data are the mean ± SD. Each dot represents one mouse. Significance (P) was calculated with unpaired t-test except for (e) (one-way ANOVA) and (f)-(g) (2way ANOVA). *: P ≤ 0.5; **: P ≤ 0.01; ***: P ≤ 0.001; ****: P ≤ 0.0001.

Supplementary Figure 4. CITE-seq antibody-derived tag (ADT) signals identifies FoB and MZB from total splenic B cells.
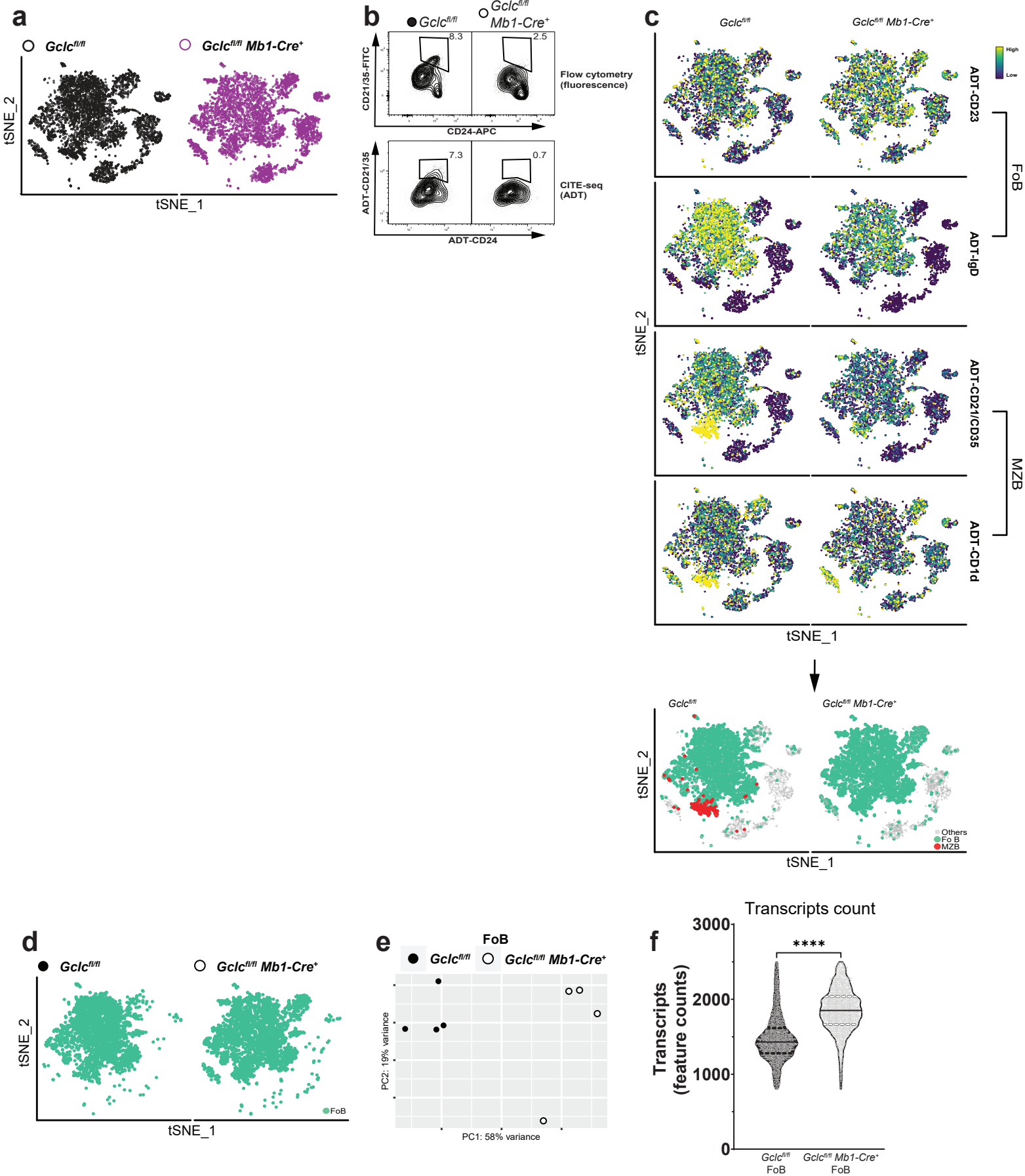
Supplementary Figure 4. CITE-seq antibody-derived tag (ADT) signals identifies FoB and MZB from total splenic B cells.

(**a**) tSNE distribution of single cell transcriptomes of FACS sorted splenic B cells from of $Gclc^{fl/fl}$ and $Gclc^{fl/fl}$ $Mb1\text{-}Cre^+$ mice (gated as in Supplementary Figure 1b). (**b**) Comparison of FACS (fluorescence) and CITE-seq signal (ADT) for the detection of MZB in $Gclc^{fl/fl}$ and $Gclc^{fl/fl}$ $Mb1\text{-}Cre^+$ mice. (**c**) Top: tSNE plots comparing ADT signals for FoB (top) and MZB (bottom) markers among splenic B cells from $Gclc^{fl/fl}$ and $Gclc^{fl/fl}$ $Mb1\text{-}Cre^+$ mice. Bottom: SCINA assignments of FoB (green) and MZB (red) from $Gclc^{fl/fl}$ and $Gclc^{fl/fl}$ $Mb1\text{-}Cre^+$ mice. (**d**) SCINA assignments of FoB from $Gclc^{fl/fl}$ and $Gclc^{fl/fl}$ $Mb1\text{-}Cre^+$ mice used for downstream analyses. (**e**) PCA plot showing distinct patterns of $Gclc^{fl/fl}$ and $Gclc^{fl/fl}$ $Mb1\text{-}Cre^+$ FoB transcriptomes (n = 4 mice/genotype). (**f**) Number of detected gene transcripts per cell in $Gclc^{fl/fl}$ and $Gclc^{fl/fl}$ $Mb1\text{-}Cre^+$ FoB. In contour plots numbers represent percentages of the cells gated. Data are pooled from 4 mice/genotype. Solid line, median; dashed lines, 1st and 3rd quartiles. Data are the mean ± SD. Significance (P) was calculated with unpaired t-test. ****: P ≤ 0.0001.

Supplementary Figure 5. Protein synthesis is enhanced in *Gclc*-deficient FoB, similarly to *Gclc*-sufficient MZB.
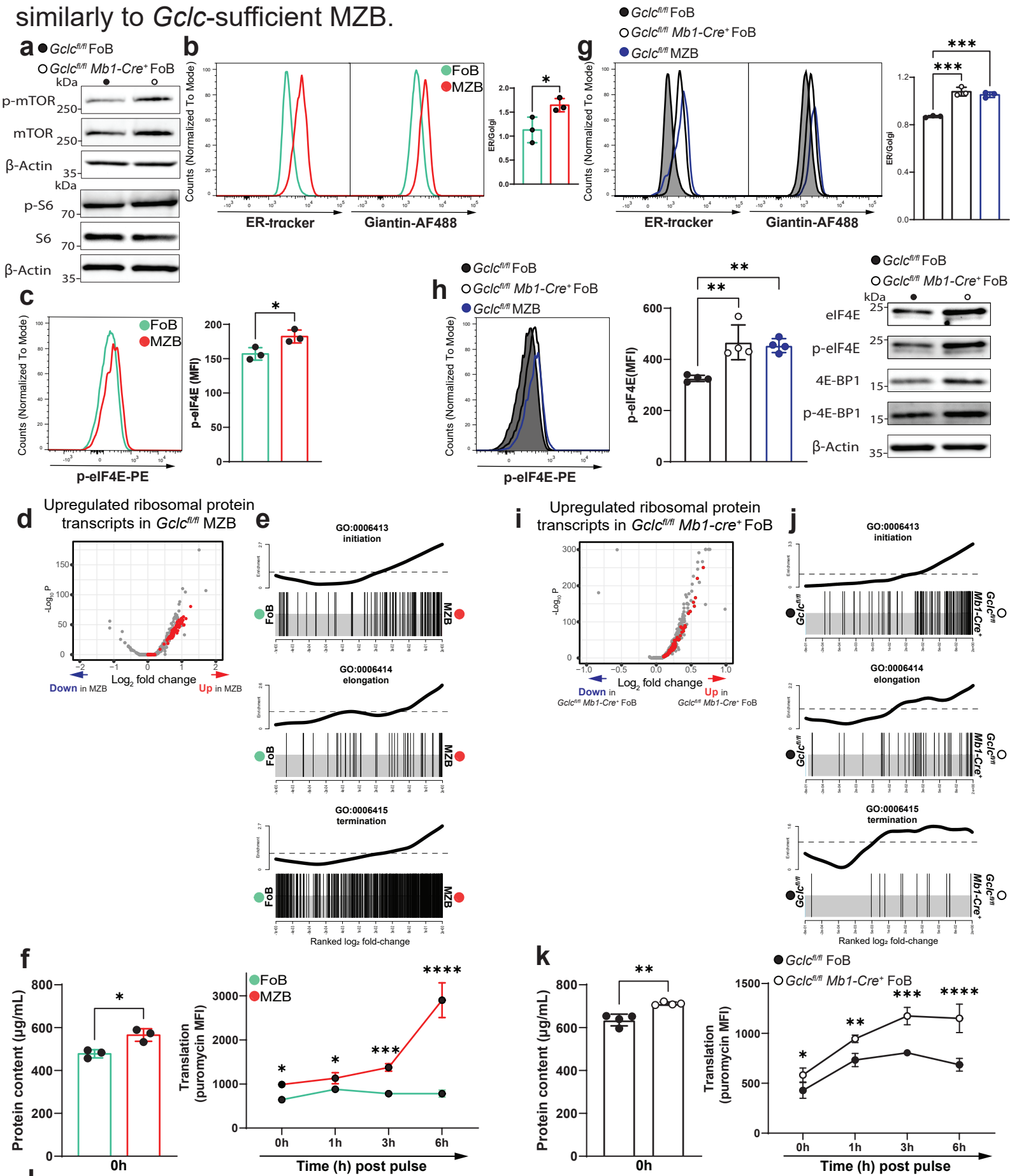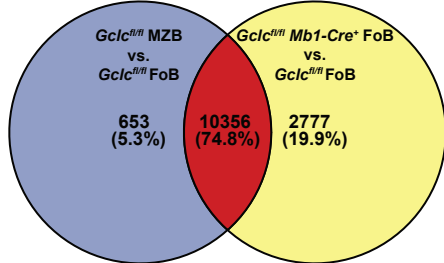
Supplementary Figure 5. Protein synthesis is enhanced in *Gclc*-deficient FoB, similarly to *Gclc*-sufficient MZB.

(**a**) Representative blot of p-mTOR, total mTOR and p-S6, total S6 proteins from total cell lysis of *Gclc*^{fl/fl} and *Gclc*^{fl/fl} *Mb1-Cre*⁺ FoB is shown. (**b-c**) Representative histogram (left) and quantitation (right) of immunostaining to detect ER-tracker and Giantin (b) and p-eIF4E (c) in B6 FoB and MZB (gated as in Supplementary Figure 1a) (n = 3 animals examined over 3 independent experiments). (**d**) Volcano plot of genes differentially expressed in *Gclc*^{fl/fl} MZB and FoB determined as in Fig. 1i. Red dots indicate upregulated ribosomal-related transcripts. Data represent up- and downregulation of MZB vs. FoB transcripts among total transcripts pooled from 4 *Gclc*^{fl/fl} mice. (**e**) Barcode plots showing transcripts from the GO:0006413, GO:0006414 and GO:0006415 gene lists that were enriched in *Gclc*^{fl/fl} MZB vs. FoB. (**f**) Protein quantitation from resting B6 0.5×10^6 cells FoB and MZB (left) and protein translation at the indicated times measured as puromycin MFI after puromycin pulse-chase of B6 FoB and MZB upon stimulation with anti-IgM, CD40 ligand and IL-4 or LPS (n = 3 animals examined over 3 independent experiments). (**g-k**) Same analyses as shown in (b-d) but comparing *Gclc*^{fl/fl} versus *Gclc*^{fl/fl} *Mb1-Cre*⁺ FoB. (g) and (h) (n = 3 animals examined over 3 independent experiments) show comparison of *Gclc*^{fl/fl} and *Gclc*^{fl/fl} *Mb1-Cre*⁺ FoB, including *Gclc*^{fl/fl} MZB as control (gated as in Supplementary Figure 1a). In (h) a representative blot of eIF4E, p- eIF4E, 4E-BP1 and p-4E-BP1 proteins from total cell lysis of *Gclc*^{fl/fl} and *Gclc*^{fl/fl} *Mb1-Cre*⁺ FoB is shown. (**j**) Venn diagrams show the percentages and numbers of transcripts overlap (red) of total differentially expressed (DE) genes between the DE analysis *Gclc*^{fl/fl} MZB vs. FoB (blue) and *Gclc*^{fl/fl} *Mb1-Cre*⁺ FoB vs *Gclc*^{fl/fl} FoB (yellow). Data are the mean ± SD. Each dot represents one mouse in (b), (e), (g) and (h). one transcript (d) and (i), mean of duplicates from 3 mice in (f, right) and (k, right) (n = 3 animals examined over 3 independent experiments). Significance (P) was calculated with unpaired t-test or one-way ANOVA test in (g)-(h) and 2way ANOVA in (f)-(k). *: $P \leq 0.05$; ***: $P \leq 0.001$.

Supplementary Figure 6. Impaired mitochondrial metabolism increases basal glycolysis in GSH-deficient FoB.
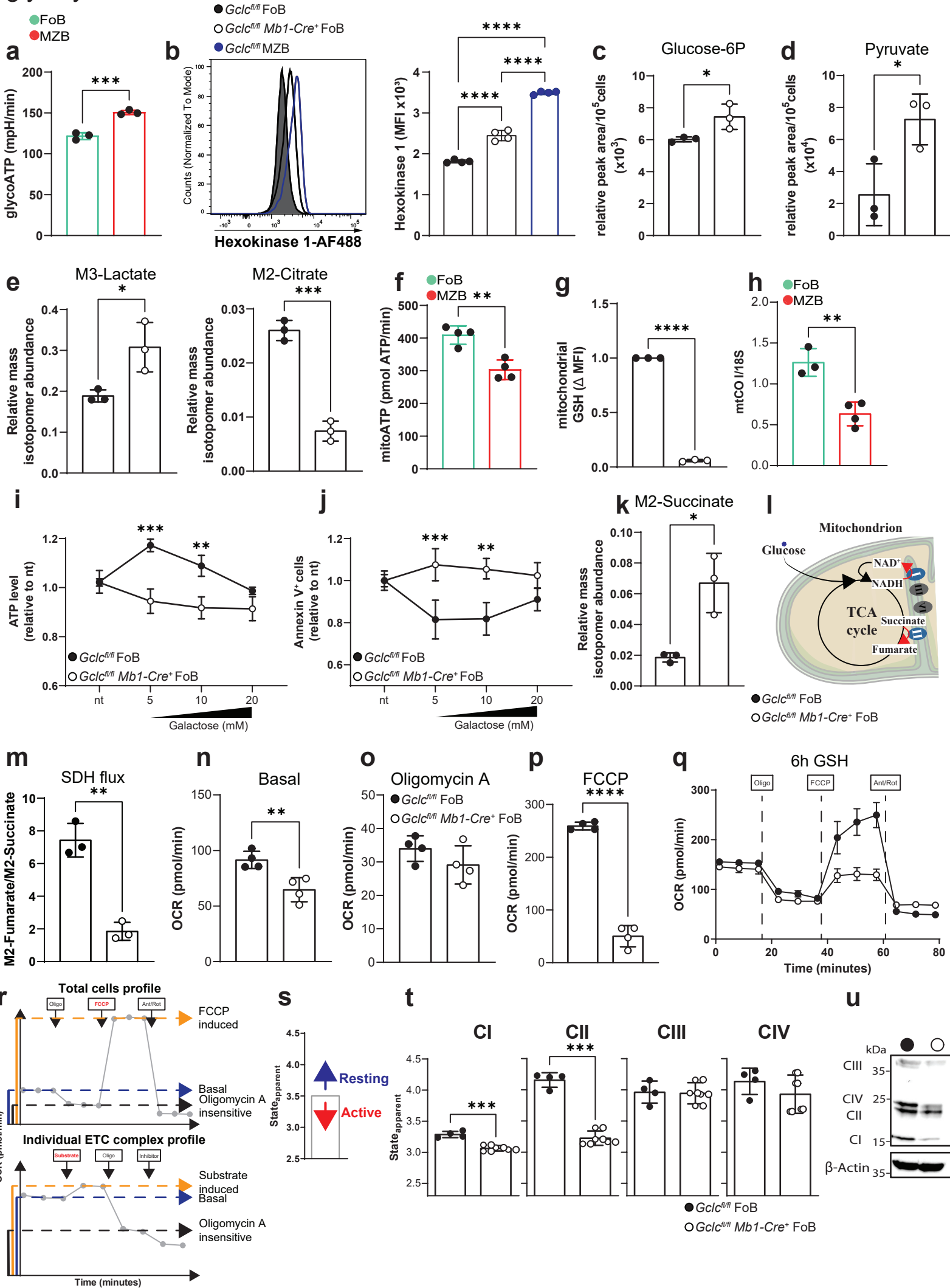
Supplementary Figure 6. Impaired mitochondrial metabolism increases basal glycolysis in GSH-deficient FoB.

(**a**) Seahorse quantitation of glycolysis-derived ATP in resting B6 FoB and MZB (n = 3 animals examined over 2 independent experiments). (**b**) Representative histogram (left) and quantitation (right) of immunostaining to detect Hexokinase-1 of $Gclc^{fl/fl}$ and $Gclc^{fl/fl}$ $Mb1$-Cre^+ FoB, including $Gclc^{fl/fl}$ MZB as control (gated as in Supplementary Figure 1a) (n = 4 animals examined over 3 independent experiments). (**c-d**) Quantitation of intracellular glucose-6P (c) and Pyruvate (d) level measured by LC-MS in resting $Gclc^{fl/fl}$ and $Gclc^{fl/fl}$ $Mb1$-Cre^+ FoB (n = 3 animals examined over 2 independent experiments). (**e**) Mass isotopomeric distribution (MID) of M3-lactate (left) and M2-Citrate (right) in $Gclc^{fl/fl}$ and $Gclc^{fl/fl}$ $Mb1$-Cre^+ FoB that were incubated with ^{13}C-glucose and assayed at 5h post-activation with anti-IgM, CD40 ligand and IL-4 (n = 3 animals examined over 2 independent experiments). (**f**) Seahorse quantification of mitochondrial-derived ATP in resting B6 FoB and MZB (n = 3 animals examined over 2 independent experiments). (**g**) Flow-cytometry-based quantitation of monobromobimane (MBB) for the detection of GSH in purified Tom20$^+$ mitochondria from $Gclc^{fl/fl}$ and $Gclc^{fl/fl}$ $Mb1$-Cre^+ FoB (gated as in Supplementary Figure 1a) (n = 3 animals examined over 2 independent experiments). (**h**) Mitochondrial mass quantitation [ratio between mitochondrial cytochrome c oxidase subunit I (CO I) and nuclear 18S ribosomal RNA] as determined by RT-qPCR of DNA from B6 FoB and MZB (n = 3-4 animals examined over 3 independent experiments). (**i, j**) Normalized ATP levels (RLU) (i) and percentage of Annexin V-expressing cells (j), in $Gclc^{fl/fl}$ and $Gclc^{fl/fl}$ $Mb1$-Cre^+ FoB after 5h incubation with the indicated concentrations of galactose (n = 3 animals examined over 2 independent experiments). (**k**) MID of M2-succinate in $Gclc^{fl/fl}$ and $Gclc^{fl/fl}$ $Mb1$-Cre^+ FoB at 5h post-activation determined as in Fig. 5e (n = 3 animals examined over 2 independent experiments). (**l**) Ratio of M2-Fumarate/M2-succinate in $Gclc^{fl/fl}$ and $Gclc^{fl/fl}$ $Mb1$-Cre^+ FoB that were incubated with ^{13}C-glucose and assayed at 5h post-activation (n = 3 animals examined over 2 independent experiments). (**m**) Complex I and II (CI and CII) reactions (red arrows) contribute to the enzymatic series of the TCA cycle within the mitochondria. (**n-p**) Quantitation of the OCR data in Fig. 6b at baseline (n) and upon treatment with oligomycin A (o) or FCCP (p) (n = 3-4 animals examined over 5 independent experiments). (**q**) Seahorse quantitation of OCR of $Gclc^{fl/fl}$ and $Gclc^{fl/fl}$ $Mb1$-Cre^+ FoB activated for 6h with anti-IgM, CD40 ligand and IL-4 and treated with 5mM GSH (n = 3-4 animals examined over 2 independent experiments).

Supplementary Figure 7. *In vivo* MZB-dependent antibody response and *in vitro* FoB activation properties are defective in *Gclc*-depleted mice.
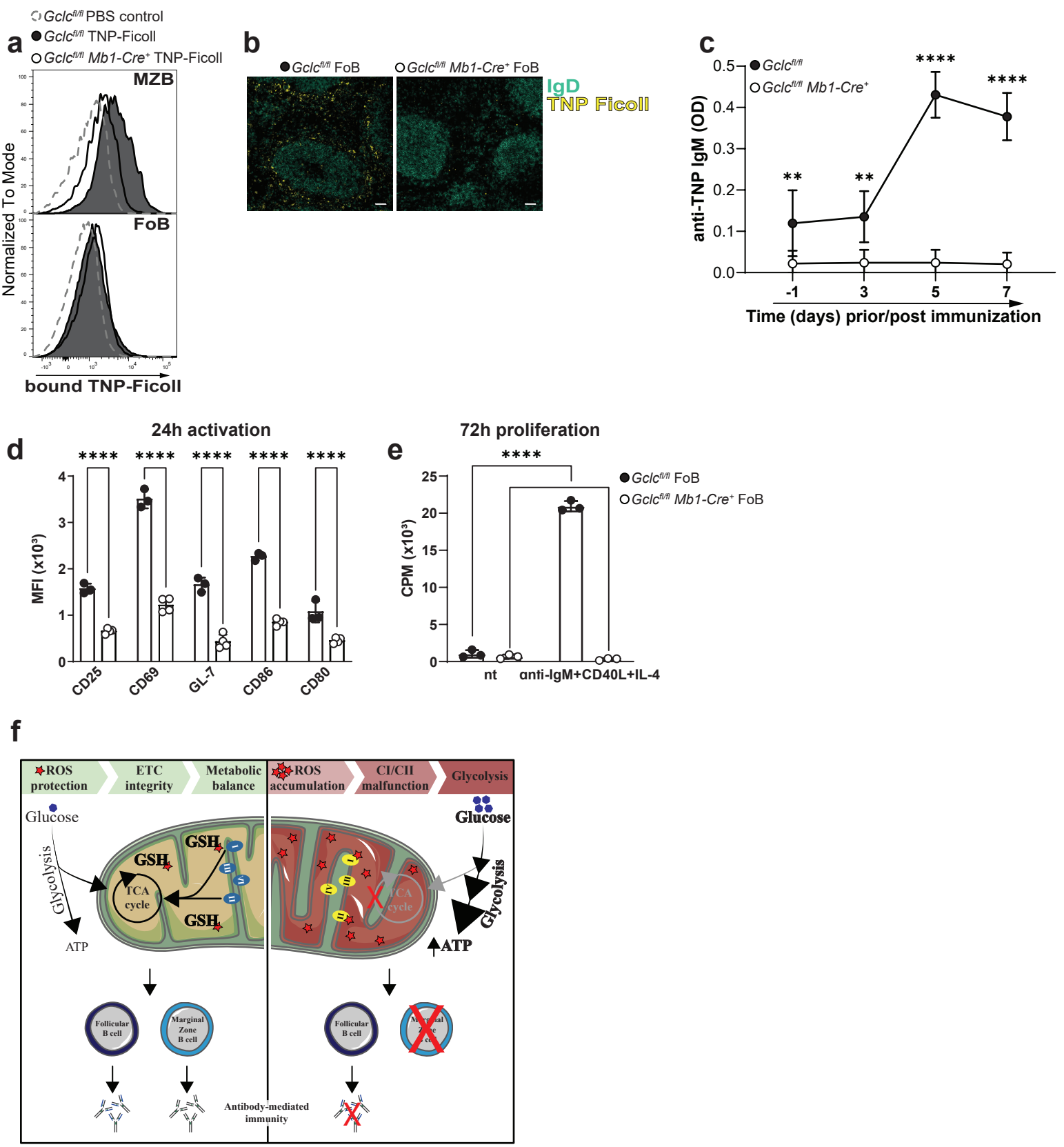
Supplementary Figure 7. *In vivo* **MZB-dependent antibody response and** *in vitro* **FoB activation properties are defective in** *Gclc***-depleted mice.**

(**a**) Representative histogram of TNP capture by *Gclc*$^{fl/fl}$ and *Gclc*$^{fl/fl}$ *Mb1-Cre*$^+$ MZB and FoB (gated as in Fig. 2e) as measured by FACS (gated as in Supplementary Figure 1a) (n = 3 animals examined over 3 independent experiments). (**b**) Representative immunofluorescence staining to detect IgD (green) and TNP-Ficoll (yellow) in spleen follicles resected from one *Gclc*$^{fl/fl}$ and one *Gclc*$^{fl/fl}$ *Mb1-Cre*$^+$ mouse at 30min after *i.v.* injection of TNP-Ficoll. Scale bars, 50 µm (n = 3 animals examined over 3 independent experiments). (**c**) Titers of anti-TNP IgM as measured by ELISA in serum of *Gclc*$^{fl/fl}$ and *Gclc*$^{fl/fl}$ *Mb1-Cre*$^+$ mice at the indicated time points after *i.p.* injection of TNP-Ficol (n = 4 animals examined over 3 independent experiments). (**d-e**) Flow cytometry expression (MFI) of surface markers after 24h activation (d) (n = 3 animals examined over 2 independent experiments) and 3H-thymidine incorporation after 72h (e) of *Gclc*$^{fl/fl}$ and *Gclc*$^{fl/fl}$ *Mb1-Cre*$^+$ FoB with anti-IgM, CD40 ligand and IL-4 (n = 3 animals examined over 2 independent experiments). (**f**) Control of mitochondrial reactive oxygen species by the antioxidant glutathione (GSH) has a subset-specific role in murine B cells. GSH is identified as non-redundant antioxidant for the correct function of the electron transport chain, and it is required for antibody-mediated humoral immunity. Data are the mean ± SD. Each dot represents one mouse except for (c) (mean of duplicates from 4 mice). Data shown are representative of ≥3 independent experiments with 3-4 mice/group. Significance (P) was calculated with 2way ANOVA. **: P ≤ 0.01; ***: P ≤ 0.0001.